JGR Oceans

RESEARCH ARTICLE
10.1029/2025JC023638

Microbial Controls on Carbon Pump Partitioning in the Subtropical North Atlantic: Stoichiometry and Nutrient Limitation Across a Basin-Scale Transect

Lukas Marx[1,2,3], **Edward Mawji**[4], **Thierry Cariou**[5], **B. B. Cael**[4,6], **Michelle Hale**[1], and **Sarah Reynolds**[1]

[1]School of the Environment and Life Sciences, University of Portsmouth, Portsmouth, UK, [2]Department of Chemistry and Geochemistry, Woods Hole Oceanographic Institution, Woods Hole, MA, USA, [3]Röst Marine Research Center, Reykjavik, Iceland, [4]National Oceanography Centre, Southampton, UK, [5]IRD, Unité d'Appui et de Recherche (UAR) Instrumentation, Moyens Analytiques, Observatoires en Géophysique et Océanographie (IMAGO), Brest, France, [6]Department of Geophysical Sciences, University of Chicago, Chicago, IL, USA

Key Points:

- Strong stratification (~125 m mixed layer depth) and deep nutriclines (>180 m) restrict nutrient resupply across the North Atlantic Subtropical Gyre
- *Prochlorococcus*-dominant showed elevated C:P, indicating phosphorus limitation in the gyre interior
- Eastern boundary waters show elevated C:P and higher productivity, reflecting reduced P limitation and enhanced exports

Supporting Information:

Supporting Information may be found in the online version of this article.

Correspondence to:

L. Marx,
lukas.marx@whoi.edu

Citation:

Marx, L., Mawji, E., Cariou, T., Cael, B. B., Hale, M., & Reynolds, S. (2026). Microbial controls on carbon pump partitioning in the subtropical North Atlantic: Stoichiometry and nutrient limitation across a basin-scale transect. *Journal of Geophysical Research: Oceans*, *131*, e2025JC023638. https://doi.org/10.1029/2025JC023638

Received 21 OCT 2025
Accepted 24 APR 2026

Author Contributions:

Conceptualization: Lukas Marx, Sarah Reynolds
Data curation: Lukas Marx, Edward Mawji, Thierry Cariou
Formal analysis: Lukas Marx, Edward Mawji, Thierry Cariou, B. B. Cael, Sarah Reynolds
Funding acquisition: Michelle Hale, Sarah Reynolds
Investigation: Lukas Marx, Edward Mawji, Thierry Cariou, B. B. Cael, Sarah Reynolds
Methodology: Lukas Marx, Edward Mawji, Thierry Cariou, B. B. Cael, Sarah Reynolds

Abstract

The subtropical North Atlantic is a key region for ocean carbon cycling despite its relatively small spatial extent. Here we present a high-resolution transect (23°–27°N; ~2° longitude spacing) across the North Atlantic Subtropical Gyre, integrating physical, chemical, and microbial observations to examine how hydrography and nutrient limitation structure organic matter stoichiometry and carbon pump partitioning. The region was strongly stratified, with a mean mixed layer depth of 125 ± 25 m deep nutriclines (>180 m), limiting nutrient resupply to surface waters in the gyre interior. Boundary regions influenced by western boundary currents and eastern upwelling exhibited higher nutrient availability and distinct microbial communities. Across this gradient, particulate and dissolved organic matter stoichiometry varied systematically with nutrient supply and microbial structure. Particulate organic matter exhibited elevated C:P and N:P ratios in the gyre interior, consistent with stronger phosphorus limitation under *Prochlorococcus*-dominated conditions, while boundary regions approached Redfield-like stoichiometry. Dissolved organic matter showed a similar spatial structure, with higher inferred C*:N and C*:P ratios in the interior relative to the margins. C* was derived from dissolved nitrogen and phosphorus using literature-based stoichiometric relationships and evaluated across multiple endmember assumptions. Although absolute values varied, spatial patterns remained consistent, indicating robust gradients despite stoichiometric uncertainty. Statistical analyses identified phosphorus availability and microbial community composition as key predictors of organic matter stoichiometry, with particulate and dissolved pools showing differing predictability. Together, these results suggest strong coupling between stratification, nutrient supply, microbial community structure, and carbon pump partitioning across the subtropical North Atlantic.

Plain Language Summary

The subtropical North Atlantic plays a major role in storing carbon from the atmosphere, even though it covers only a small part of the global ocean. This study used detailed measurements across the region to understand how temperature, ocean circulation, and nutrient availability influence planktonic organisms that drive carbon cycling. In the nutrient-poor central gyre system, microscopic cyanobacteria like *Prochlorococcus* dominate and produce organic matter that is largely recycled within the upper ocean or transformed into long-lived dissolved form. In contrast, the nutrient-rich edges of the gyre support a more diverse plankton community that contributes more to sinking particles exported to the deep ocean. Together, these processes shape the balance between two key carbon storage mechanisms: the biological carbon pump, which transports carbon to depth via particles, and microbial processes that transform and retain dissolved organic carbon in surface waters. As climate change strengthens ocean stratification and reduces nutrient supply to surface waters, the balance between these pathways may shift. Such changes could alter how efficiently the subtropical North Atlantic stores carbon and regulates atmospheric CO_2.

1. Introduction

The North Atlantic, though smaller than other ocean basins, plays a disproportionate role in the global carbon cycle, accounting for a large fraction of oceanic CO_2 uptake and export production (Friedlingstein et al., 2024; Reay et al., 2008). Within this basin, the subtropical North Atlantic gyre (NASG) is a key site of carbon sequestration, strongly shaped by Gulf Stream transport and the Atlantic Meridional Overturning Circulation

Project administration: Michelle Hale, Sarah Reynolds
Resources: Michelle Hale, Sarah Reynolds
Supervision: B. B. Cael, Michelle Hale, Sarah Reynolds
Validation: Lukas Marx, Edward Mawji, Thierry Cariou, B. B. Cael, Michelle Hale, Sarah Reynolds
Visualization: Lukas Marx
Writing – original draft: Lukas Marx
Writing – review & editing: Lukas Marx, Edward Mawji, Thierry Cariou, B. B. Cael, Michelle Hale, Sarah Reynolds

(AMOC) (Primeau, 2005; Ridge & McKinley, 2020). Permanent stratification and oligotrophy characterize the NASG, where high dust deposition can stimulate diazotrophic N_2-fixation but phosphorus supply remains scarce, leading to widespread P-(co)limitation (Jickells et al., 2005; Macovei et al., 2019; Mather et al., 2008).

Planktonic organisms are central to carbon cycling in this system. Productivity at the nutrient-rich boundaries of the gyre supports diverse assemblages, while the oligotrophic interior is dominated by small cyanobacteria such as *Prochlorococcus* and *Synechococcus*, which together contribute a large fraction of chlorophyll *a* in the region (Flombaum et al., 2013; Hickman et al., 2010). Particulate organic matter (POM) produced by these communities underpins the biological carbon pump, although much of this material is rapidly remineralized in the upper ocean or released as dissolved organic matter (DOM). In oligotrophic systems, long-term carbon storage is increasingly thought to be linked to microbial processing of DOM and the transformation of fresh organic matter into more persistent forms that accumulate in the ocean interior (Guidi et al., 2016; Jiao et al., 2010; Polimene et al., 2017).

The stoichiometry of POM and DOM provides important constraints on these processes. POM often approximates Redfield proportions (106:16:1), whereas DOM is typically more carbon-rich, particularly in its more refractory fractions, reflecting both microbial processing and nutrient limitation (Browning & Moore, 2023; Hopkinson & Vallino, 2005; Liang et al., 2023; Moore et al., 2013). As a result, shifts in plankton community structure — from nutrient-replete boundary systems to cyanobacteria-dominated gyre interiors — are expected to influence both particulate export and DOM accumulation and transformation.

Recent studies have highlighted the coupling between plankton ecology, nutrient availability, and carbon cycling across the Atlantic: Microbial interactions involving *Prochlorococcus* can strongly influence ecosystem function and carbon processing (Cai et al., 2024), while regional variability in POM stoichiometry reflects differences in nutrient supply and community composition (Fagan et al., 2024). Nutrient-ratio budget approaches further suggest that subtropical gyres are maintained by tight internal recycling under chronic phosphorus stress (Masuda et al., 2023; Xiang et al., 2023). At finer scales, temporal partitioning of nutrient acquisition strategies enables microbial communities to sustain productivity under low-P conditions (Muratore et al., 2024), while global models indicate that phytoplankton nutrient plasticity will play an important role in regulating future carbon cycling (Kwon et al., 2022). Together, these studies emphasize that plankton physiology and nutrient availability jointly structure organic matter production and transformation, with implications for the relative roles of particulate export and microbial recycling.

Here, we present a high-resolution west-east transect across the subtropical North Atlantic (between 23° and 27°N) with sampling spaced approximately every 2° longitude (Figure 1), integrating physical, chemical, and microbial observations to examine how hydrography and nutrient availability shape plankton communities, organic matter stoichiometry, and carbon pump partitioning. We test three working hypotheses relating to: (a) community structure shifts from nutrient-replete boundary assemblages dominated by *Synechococcus* and picoeukaryotes to *Prochlorococcus*-dominated assemblages in the oligotrophic interior of the NASG; (b) POM and DOM elemental ratios vary systematically along the gradient, with elevated C:P and N:P in the interior reflecting stronger nutrient limitation and altered microbial processing; and (c) basin-scale variability in organic matter stoichiometry can be statistically related to environmental and microbial drivers, including nutrient concentrations, cyanobacterial abundance, and heterotrophic community structure. To quantify these relationships, we applied a multi-tiered statistical framework integrating stepwise regression, random forest models, mixed-effect models, and cross-validation. This approach allows identification of key predictors while accounting for spatial structure and model uncertainty. By combining these complementary methods, we assess the relative importance of environmental and biological controls on organic matter stoichiometry and microbial community structure across the NASG, and explore how these relationships vary along a strong hydrographic and nutrient gradient.

2. Materials and Methods

2.1. Sampling and Analyses

Sampling was conducted during the RRS James Cook cruise JC191 (19 January–1 March 2020) along a west–east transect centered near 24°N (spanning ~23°–27°N depending on station location) from Port Everglades, USA, to Santa Cruz de Tenerife, Spain, occupying GO-SHIP reference section A05 (Figure 1).

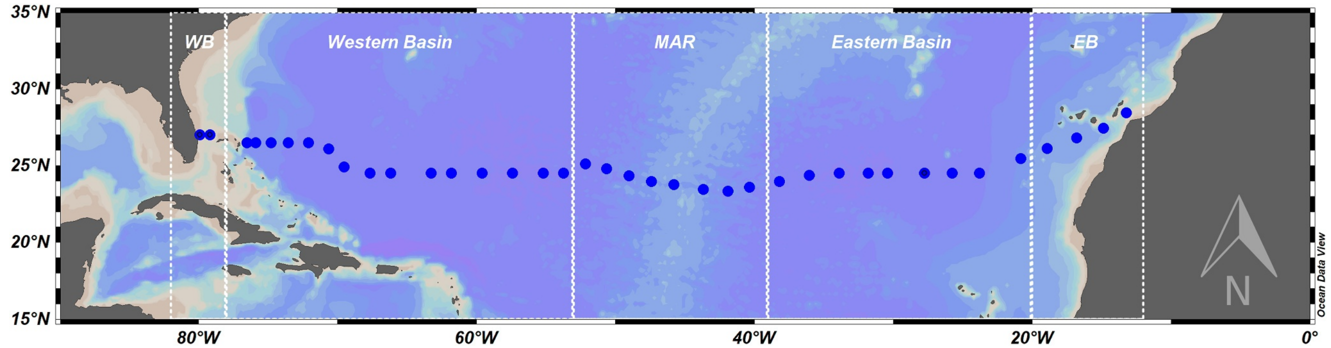

Figure 1. Spatial map of the study region in the subtropical North Atlantic (centered at 24°N (23°–27°N)). Blue dots indicate sampling locations (38 out of 135 CTD stations occupied). White sections indicate the defined subregions: WB = Western Boundary, Western Basin, MAR = Mid-Atlantic Ridge, Eastern Basin, and EB = Eastern Boundary, based on temperature-salinity signatures.

Out of 135 stations, 38 were sampled for ecological and biogeochemical parameters at six depths (max. 375 m) spanning the euphotic zone. Water (5 L) was collected from Niskin bottles mounted on a CTD rosette (Seabird 911, equipped with AQUAtracka III fluorometer). Subsamples were taken for dissolved inorganic nutrient analysis (NO_3^-, NO_2^-, PO_4^{3-}, and $Si(OH)_4$), dissolved and POM analysis (carbon (C), nitrogen (N), and phosphorus (P)), chlorophyll *a* analysis (hereafter Chl *a*), and microbial community composition (cyanobacteria *Prochlorococcus* and *Synechococcus*, picoeukaryotes <20 μm, and heterotrophic high-nucleic-acid (Hnac) and low-nucleic-acid (Lnac) containing bacteria) via flow cytometric determination.

Dissolved inorganic nutrients (NO_3^-, NO_2^-, Si (determined as $Si(OH)_4$), and PO_4^{3-}) were analyzed on board within 8 hr after collection using a SEAL AA3 autoanalyzer following GO-SHIP protocols (Becker et al., 2020). Precision was assessed using CRMs (KANSO), with long-term standard deviations of 0.011 μmol L^{-1} (NO_3^-), 0.004 μmol L^{-1} (NO_2^-), 0.033 μmol L^{-1} (Si), and 0.003 μmol L^{-1} (PO_4^{3-}).

Samples for dissolved organic phosphorus (DOP) were obtained from filtrates passing through GF/F filters for collection of dissolved nutrients, and stored frozen (−20°C) until analysis by high-temperature persulfate oxidation (following Lomas et al., 2010; Davis et al., 2014, 2019). Total dissolved phosphorus was measured colorimetrically, and DOP was calculated as TDP–PO_4^{3-}. Oxidation efficiencies were monitored with nucleotide standards (ADP, PEP, DGMP and ATP). Long-term reproducibility for DOP was 0.004 μmol L^{-1}. Dissolved organic nitrogen (DON) was analyzed by high-temperature catalytic oxidation (Dickson et al., 2007) using KHP/glycine calibration and CRMs for accuracy; relative uncertainty was 0.12 μmol L^{-1}.

Particulate organic carbon (POC), nitrogen (PN), and phosphorus (PP) were collected on pre-combusted GF/F filters (2 L filtered) and stored frozen (−20°C). Although technically total particulate nitrogen is measured, with the scope of a basin-spanning transect, we present it as particulate organic nitrogen (PON), assuming negligible contribution from particulate inorganic nitrogen, which is typical for oligotrophic open-ocean environments. Similarly, PP represents particulate organic phosphorus. POC and PON were analyzed on a Flash2000 elemental analyzer after vapor-phase decarbonization, with analytical precision of ±0.28 μg L^{-1} (POC) and ±0.36 μg L^{-1} (PON). PP was determined after combustion and acid extraction as dissolved inorganic phosphorus on a SEAL AA500 autoanalyzer (Davis et al., 2014) with a relative uncertainty of 0.03 μmol L^{-1}, and then converted into PP in μg L^{-1}.

Chl *a* was quantified using the JGOFS acidification method (Knap et al., 1996). Filters (200 mL samples collected on GF/F filters) were extracted in 90% acetone at −20°C and analyzed fluorometrically (Turner AU-10). Accuracy was within 5% of reference standards. Measurements were cross-calibrated with in situ fluorometer data.

For microbial counts, 4 mL of unfiltered seawater was fixed with glutaraldehyde (0.5% final concentration) and stored at −80°C. Autotrophic cyanobacteria (*Prochlorococcus*, *Synechococcus*) and picoeukaryotes (<20 μm) were enumerated directly, while heterotrophic bacteria (Hnac and Lnac) were stained with SYBR Green I DNA dye prior to analysis on a CyFlow Cube 8 cytometer (Sysmex) following Tarran and Bruun (2015). Results were validated using fluorescent beads (diameter 3.6 μm, Beckman Coulter) as internal standards.

2.2. Derived Variables

Mixed layer depth (MLD) was defined from CTD temperature profiles as the depth at which the temperature decreased by 1°C from the surface (S. E. Reynolds et al., 2007). Such an arguably conservative temperature threshold provides a robust indicator of surface stratification, specifically for subtropical oligotrophic waters where density differences are often small, and allows a consistent basis for cross-basin and global comparison (de Boyer Montégut et al., 2004; Kara et al., 2003). Nutricline depths were estimated from logarithmic fits of nutrient profiles, with Z_N ($NO_3^- \geq 2$ μmol L^{-1}) and Z_P ($PO_4^{3-} \geq 0.1$ μmol L^{-1}) following Dave et al. (2015). Analytically derived concentrations and elemental stoichiometry were depth-integrated within the MLD. Density (σ_θ) was calculated from the CTD temperature and salinity to identify water masses. The depth of the deep chlorophyll maximum (DCM) was determined from in situ fluorescence profiles.

The metabolic state (AC:HC ratio) of the microbial community was estimated as the ratio of autotrophic to heterotrophic cell counts following Calvo-Díaz et al. (2011):

$$\text{Metabolic state} = \frac{\text{Pro} + \text{Syn} + \text{Picoeuks}}{\text{Hnac} + \text{Lnac}}$$

The quasi-conservative tracer N* was calculated to assess the imprint of nitrogen fixation following Gruber and Sarmiento (1997):

$$\text{N}^* = \left(\text{NO}_3^- - 16\text{PO}_4^{3-} + 2.90\right) \times 0.87$$

Values >2 μmol L^{-1} are commonly interpreted as indicative of excess nitrogen relative to Redfield proportions and are commonly used as a qualitative indicator of potential N_2-fixation influence in the thermocline of the subtropical North Atlantic, although alternative physical and biogeochemical processes may also contribute (Gruber & Sarmiento, 1997).

Samples for DOC could not be used due to contamination (DOC > 1,000 μmol L^{-1}), caused by leaching of carbon-based polymers from the vessel lids into the seawater sample, precluding reliable quantification of DOC. To provide a first-order constraint on DOM composition, we therefore derived an inferred carbon proxy (hereafter C*) from measured DON and DOP using literature-based DOM stoichiometric relationships (Liang et al., 2023).

C* was calculated independently from DON and DOP as

$$\text{C}_\text{N}^* = (\text{C} : \text{N})_\text{DOM} \times [\text{DON}]$$

$$\text{C}_\text{P}^* = (\text{C} : \text{P})_\text{DOM} \times [\text{DON}]$$

Where $(\text{C:N})_\text{DOM}$ and $(\text{C:P})_\text{DOM}$ represent assumed bulk DOM stoichiometric ratios, and [DON] and [DOP] are concentrations measured across the transect. The global mean for bulk DOM (387:26:1, C:N:P) was used as the primary reference. To reduce dependence on any single assumption, C* was defined as the mean of C*_N and C*_P estimates. Because DOM stoichiometry varies within and across environments, we assessed the sensitivity of inferred C* to alternative endmember compositions, including global semi-labile DOM (179:20:1) and regionally constrained bulk (638:43:1) and semi-labile (414:49:1) DOM stoichiometries reported specific to the NASG (Table S3 in Supporting Information S1, Liang et al., 2023). Variability across these endmember assumptions was quantified using coefficients of variation (CV, %), calculated as the standard deviation divided by the mean across all estimates per endmember scenario. We emphasize that C* represents a derived proxy rather than a direct measurement of DOC. Accordingly, C*-based DOM stoichiometries are interpreted as indicators of relative DOM compositional structure rather than absolute carbon concentrations. Uncertainty associated with assumed stoichiometry is therefore explicitly constrained and does not affect the robustness of observed basin-scale spatial patterns.

2.3. Statistical Analysis

All analyses were conducted in RStudio (v1.4.1106; R Core Team, 2022). While the full data set was not normally distributed (Shapiro–Wilk, $p < 0.05$), normality within subregions and sample size ($n = 38$) supported the use of

Table 1
Physico-Chemical Properties of Defined Subregions (Mean ± SD)

	Western boundary ($n = 2$)	Western basin ($n = 15$)	Mid-Atlantic ridge ($n = 8$)	Eastern basin ($n = 9$)	Eastern boundary ($n = 4$)
Latitude	27°N	26.5°–24.5°N	25.1°–23.3°N	24°–25.5°N	26.1°–28.4°N
Longitude	79.9°–79.2°W	76.5°–53.7°W	52.2°–40.3°W	38.2°–20.8°W	18.9°–13.2°W
Temperature [°C]	25.5 ± 0.5	24.1 ± 0.4	23.3 ± 0.3	21.8 ± 0.8	18.7 ± 0.8
Salinity [psu]	36.5 ± 0.2	37 ± 0.2	37.4 ± 0.1	37.3 ± 0.2	36.6 ± 0.1
Dissolved oxygen [μmol kg^{-1}]	199.3 ± 2.5	209.2 ± 1.5	210.2 ± 2.3	214.4 ± 3.9	228.3 ± 4.9
Density σ_θ [kg m^{-3}]	24.3 ± 0.3	25.2 ± 0.1	25.7 ± 0.1	26.1 ± 0.1	26.4 ± 0.1
MLD [m]	100 ± 51	111 ± 16	139 ± 12	141 ± 17	120 ± 46
Z_N [m]	102 ± 35	217 ± 24	203 ± 24	185 ± 29	120 ± 42
Z_P [m]	79 ± –	241 ± 28	213 ± 21	161 ± 49	67 ± 38
DCM [m]	37 ± 20	115 ± 19	141 ± 15	96 ± 51	45 ± 25

Note. Depth-integrated temperature, salinity and dissolved oxygen from CTD profiles, calculated density (σ_θ), calculated nutricline depths Z_N and Z_P, and deep chlorophyll maximum (DCM) from AQUAtracka III fluorescence profiles.

parametric tests under the central limit theorem (Kwak & Kim, 2017). We first explored the full data set using Pearson correlation (Figure S1 in Supporting Information S1). Then, for each response variable (POM C:N, DOM C*:N, and AC:HC), we defined mechanistic predictor pools informed by nutrient availability, plankton community composition, and microbial activity (Table S1 in Supporting Information S1). Predictor pools were selected to test mechanistic links between nutrient supply, microbial community structure, and temperature-regulated metabolism in structuring particulate stoichiometry, dissolved stoichiometry, and autotroph–heterotroph metabolic balance. Stepwise regressions (backward selection, maximum of five predictors) were applied to identify the most influential variable. This approach permits interpretability and the ability to highlight key drivers across multiple variables. Predictor importance was further assessed using random forest models, while linear mixed-effect models included the pre-defined subregions as a random effect to account for spatial structure. Predictor contributions were summarized across all three approaches, and the top predictors were highlighted for each response. Model outputs, including estimates, cross-validation results, and variance explained, were integrated to provide a robust assessment of the environmental and ecological drivers of organic matter stoichiometry and microbial community structure (Table S2 in Supporting Information S1).

3. Results

3.1. Hydrography of the Subtropical North Atlantic

The subtropical North Atlantic was strongly stratified, with a mean MLD of 125 ± 25 m (Table 1). Five hydrographic subregions were identified along the transect based on contrasting temperature-salinity signatures (Figure 1, Figure S2 in Supporting Information S1), and measured parameters were integrated across the MLD. Transect-wide cross-sections of temperature, salinity and dissolved oxygen cross-section are shown in Figure S3 in Supporting Information S1. The western boundary was warm (25.5 ± 0.5°C, 36.5 ± 0.2 psu), whereas the eastern boundary exhibited similar salinity (36.6 ± 0.1 psu) but substantially cooler temperatures (18.7 ± 0.8°C), resulting in higher density above the MLD ($\sigma_\theta = 26.4$). In contrast, the central gyre (Mid-Atlantic Ridge and eastern basin) displayed the highest salinities (>37.3 psu) and intermediate densities. Dissolved oxygen declined westward and correlated negatively with temperature ($r = -0.94$, $p < 0.001$) and salinity ($r = -0.72$, $p < 0.01$). Oxygen concentrations were highest in the east (>220 μmol kg^{-1}), consistent with the influence of oxygenated waters associated with upwelling and circulation processes. Together, these gradients reflect a transition from warm, oligotrophic, and highly stratified gyre waters in the western NASG to cooler, more nutrient-influenced conditions toward the eastern boundary.

3.2. Planktonic Biomass and Community Composition

Chl *a*, a proxy for phytoplankton biomass, was low across surface waters of the gyre interior (<0.1 μg L^{-1}) but increased sharply in the eastern boundary (>0.4 μg L^{-1}) (Table 2, Figure S4 in Supporting Information S1). Chl *a*

Table 2
Depth-Integrated Biological Parameters of Defined Subregions (Mean ± SD)

	Western boundary ($n = 2$)	Western basin ($n = 15$)	Mid-Atlantic ridge ($n = 8$)	Eastern basin ($n = 9$)	Eastern boundary ($n = 4$)
Chl *a* [μg L^{-1}]	0.11 ± 0.07	0.08 ± 0.03	0.11 ± 0.02	0.16 ± 0.05	0.28 ± 0.07
Prochlorococcus [10^3 cell counts mL^{-1}]	145 ± 95	102 ± 38	80 ± 21	92 ± 22	52 ± 18
Synechococcus [10^3 cell counts mL^{-1}]	26 ± 7	14 ± 14	11 ± 12	17 ± 12	39 ± 26
Picoeukaryotes [10^3 cell counts mL^{-1}]	3.1 ± 1.9	2.3 ± 0.4	2.3 ± 0.2	5.4 ± 3.2	15.1 ± 14.1
Pro:Syn ratio	5.54	7.34	7.14	5.49	1.33
Hnac [10^6 cell counts mL^{-1}]	1.4 ± 0.1	1.3 ± 1.2	1.1 ± 0.3	1.3 ± 0.2	2.2 ± 0.3
Lnac [10^6 cell counts mL^{-1}]	1.5 ± 0.1	1.4 ± 0.2	1.4 ± 0.4	2.0 ± 0.3	2.7 ± 0.3
AC:HC	0.062 ± 0.03	0.049 ± 0.02	0.041 ± 0.02	0.036 ± 0.01	0.022 ± 0.008

Note. Chl *a*, abundance of *Prochlorococcus*, *Synechococcus*, Hnac and Lnac from discrete measurements, and *Pro:Syn* ratio and AC:HC derived from these.

strongly correlated with nutrient supply ($r = 0.75$ for NO_3^-, $r = 0.88$ for PO_4^{3-}, both $p < 0.001$). The DCM was shallowest in the western (37 ± 20 m) and eastern (45 ± 25 m) boundaries and deepened in the central NASG, particularly in the western basin (>100 m) (Table 1).

Prochlorococcus dominated the phytoplankton community throughout the euphotic zone, peaking at the western boundary ($145 \pm 95 \times 10^3$ cells counts mL^{-1}) and declining eastward (Figure 2a). Abundances correlated positively with temperature ($r = 0.41$, $p < 0.05$) and negatively with nutrients ($r = -0.52$ for NO_3^-, $p < 0.01$). *Synechococcus* was largely confined to the upper 100 m, with maxima in the eastern boundary ($39 \pm 26 \times 10^3$ cell mL^{-1}), correlating positively with NO_3^- ($r = 0.46$, $p < 0.05$) and negatively with temperature ($r = -0.42$, $p < 0.05$) (Figure 2b). Picoeukaryotes followed a similar eastward increase (Figure 2c). Consequently, the *Pro:Syn* ratio was highest in the gyre interior (>5) but lowest in the eastern boundary (1.3), consistent with a shift in dominance under relatively nutrient-replete conditions (Table 2). These contrasting distributions demonstrate how nutrient availability and stratification structure cyanobacterial niches across the basin.

Heterotrophic bacteria were abundant across the transect and were dominated by low-nucleic-acid containing (Lnac) cells, which increased eastward (up to $2.7 \pm 0.3 \times 10^6$ cells counts mL^{-1}) (Figure 3b). High-nucleic-acid containing (Hnac) cells were more prevalent in productive boundary regions ($1.4 \pm 0.1 \times 10^6$ cell counts mL^{-1} in the west and $2.2 \pm 0.3 \times 10^6$ cell counts mL^{-1} in the east) (Figure 3a). Autotroph:heterotroph (AC:HC) ratios declined eastward, from 0.062 ± 0.03 in the western boundary to 0.022 ± 0.008 in the eastern boundary, driven primarily by changes in *Prochlorococcus* abundance ($r = 0.81$, $p < 0.001$) (Table 2). This decline is consistent with a shift toward relatively greater heterotrophic biomass under enhanced nutrient supply.

3.3. Nutrient Distributions

Surface waters across the NASG were strongly depleted in macronutrients (<0.1 μmol L^{-1} NO_3^-, <0.01 μmol L^{-1} PO_4^{3-}), with deep nutriclines ($Z_N = 190 \pm 44$ m, $Z_P = 190 \pm 68$ m) (Figure 4). Nutriclines were deepest in the western basin ($Z_N = 217 \pm 24$ m, $Z_P = 241 \pm 28$ m) but shoaled markedly at the eastern boundary ($Z_N = 120 \pm 42$ m, $Z_P = 67 \pm 38$ m), consistent with upwelling of nutrient-rich waters and elevated surface productivity. Temperature correlated negatively with nutrients ($r = -0.77$ for NO_3^-, $r = -0.90$ for PO_4^{3-}, both $p < 0.001$), further supporting the role of upwelled colder waters in nutrient supply.

DOM constituted the majority of the total dissolved pool, accounting for >90% of total dissolved nitrogen and phosphorus (Figure S5 in Supporting Information S1). DON concentrations were highest in the central NASG (>7 μmol L^{-1}) (Figure 5a), whereas DOP declined eastward to near depletion (<0.01 μmol L^{-1}) (Figure 5b). Consequently, total dissolved N:P ratios were highly elevated (>300 in the Mid-Atlantic Ridge region), far exceeding the Redfield ratio (Table 3). These patterns indicate strong phosphorus scarcity driving pronounced N:P imbalances.

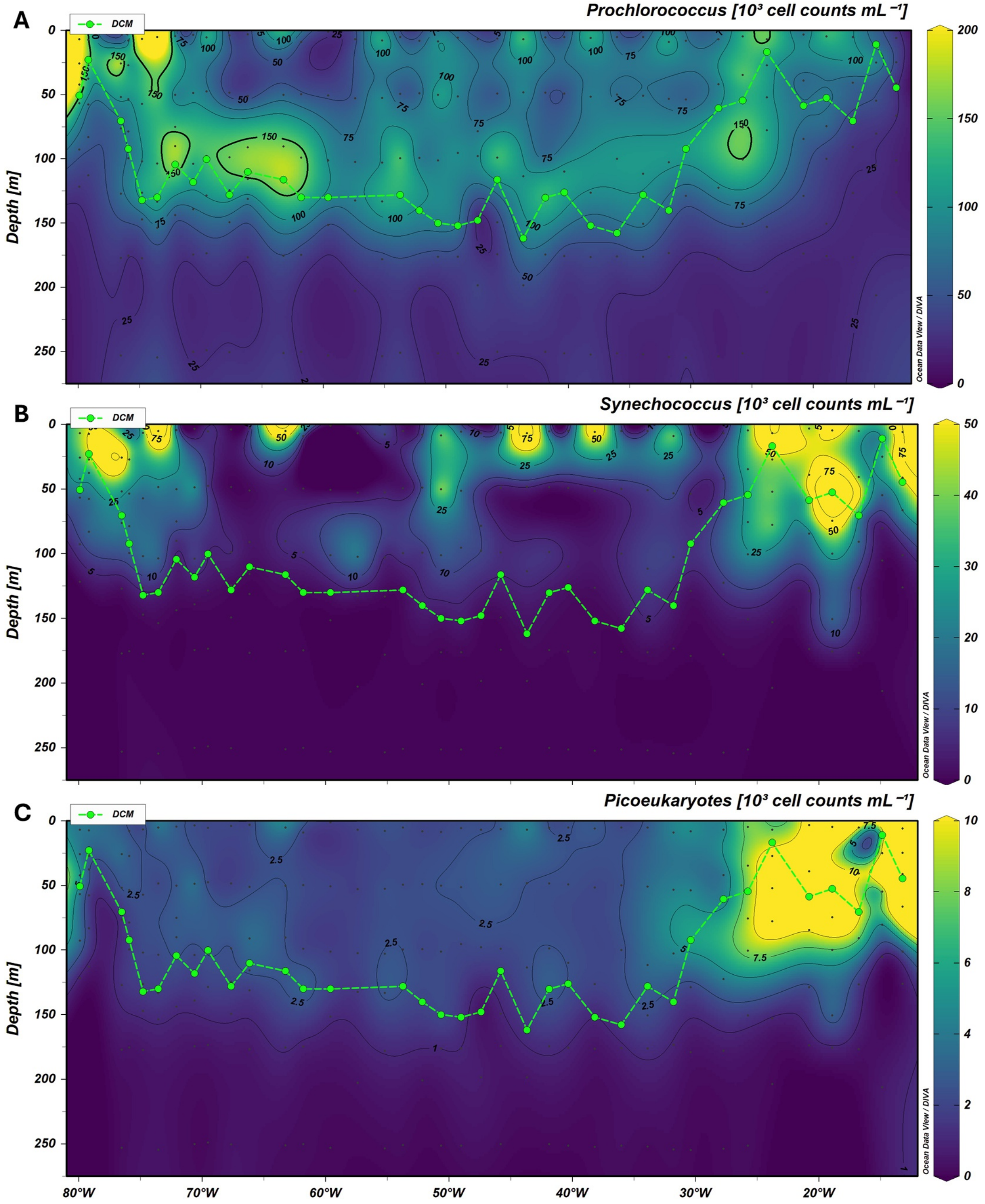

Figure 2. Abundance (10^3 cell counts mL^{-1}) and distribution of (a) *Prochlorococcus*, (b) *Synechococcus*, and (c) picoeukaryotes across the transect. Black dots indicate discrete sampling depths for flow cytometric determination and green dashed line and dots indicate deep chlorophyll maximum at each station occupied.

3.4. Particulate and Total Organic Matter

POM was concentrated within the euphotic zone and showed strong regional contrasts (Table 3). POC and PON were highest in the eastern boundary (>50 and 7.5 μg L^{-1}, respectively), reflecting enhanced productivity (Figures 6a and 6b). PP also increased sharply eastward (>0.3 μg L^{-1}) (Figure 6c), with additional peaks above the Mid-Atlantic Ridge, suggesting localized productivity enhancement. POM stoichiometry reflected nutrient availability: C:P and N:P ratios were highest in the western NASG (213 ± 45 and 44 ± 7, respectively) and declined eastward (<130 and ~20, respectively), consistent with relief of phosphorus limitation in upwelling-influenced waters (Table 3; Figure S6 in Supporting Information S1).

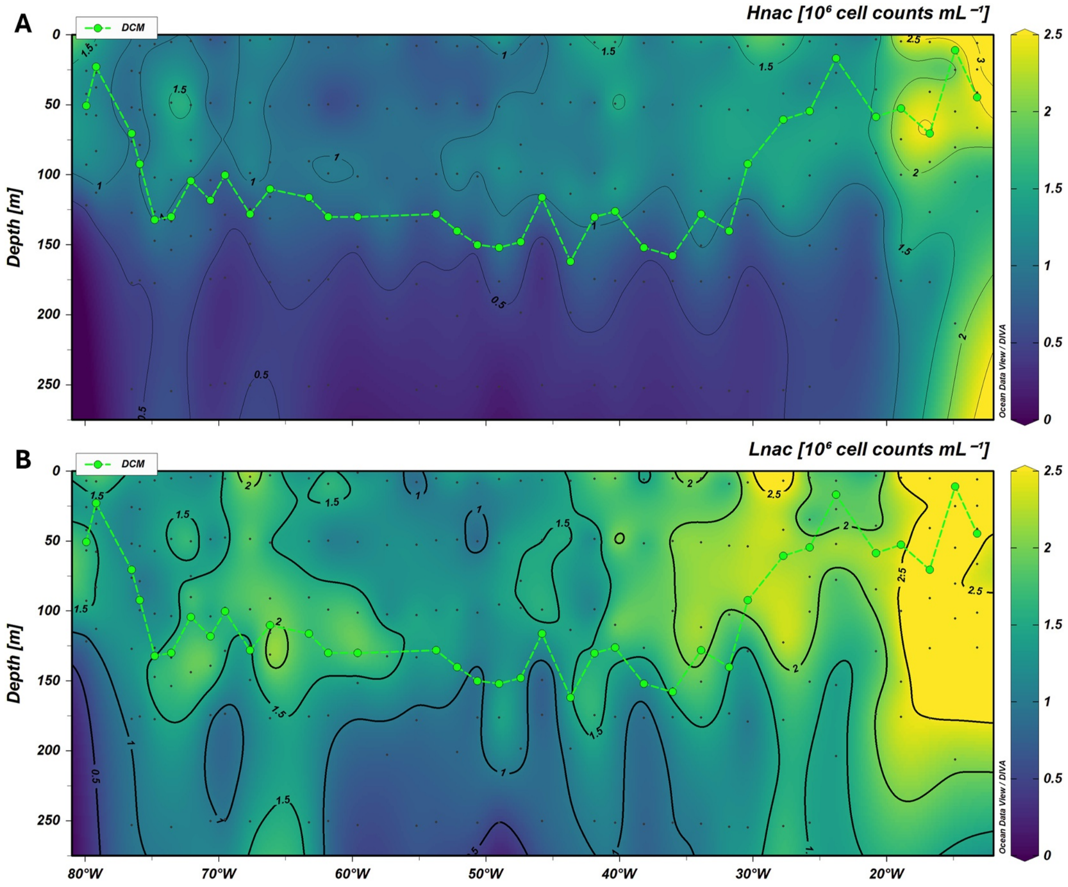

Figure 3. Abundance (10^6 cell counts mL^{-1}) and distribution of (a) Hnac and (b) Lnac heterotrophic bacteria across the transect. Black dots indicate discrete sampling depths for flow cytometric determination and green dashed line with dots indicate deep chlorophyll maximum at each station occupied.

The total organic matter pool (TOM) was dominated by DOM, particularly in the gyre interior. TOM N:P ratios reached extreme values (~260 in the Mid-Atlantic Ridge region) driven by nitrogen excess relative to phosphorus (Table 3). Together, these results suggest that DOM accumulation and chronic P limitation jointly control basin-scale organic matter stoichiometry.

3.5. Indicators of Nutrient Imbalance

The nitrogen anomaly (N*) increased with temperature ($r = 0.86$, $p < 0.001$), consistent with regions of potential diazotrophic influence (Table 3). Elevated N* coincided with high DON concentrations and extreme total organic N:P ratios, suggesting a potential role for biological nitrogen inputs in shaping basin-scale nutrient imbalances. We note, however, that N* is an indirect tracer and may also reflect physical processes such as advection of nutrient-rich waters or local remineralization (Williams et al., 2011, 2026). Accordingly, N* should be interpreted as a qualitative indicator of nitrogen excess rather than a diagnostic measure of N_2-fixation.

3.6. Statistical Identification of Drivers

Statistical modeling was used to identify environmental and biological predictors of variability in POM C:N and DOM C*:N stoichiometry, and microbial community structure (AC:HC) ratios (Table S1 in Supporting Information S1). Predictive performance for POM C:N was low overall (CV $R^2 = 0.054$), indicating substantial unexplained variability in particulate stoichiometry (Table S2 in Supporting Information S1). Across modeling approaches, no single dominant set of predictors emerged. Random forest analysis identified PO_4^{3-} concentration, Prochlorococcus abundance, and Lnac bacterial abundance as important variables. Stepwise regression similarly retained PO_4^{3-} as a weak but consistent predictor, alongside Prochlorococcus in some model iterations.

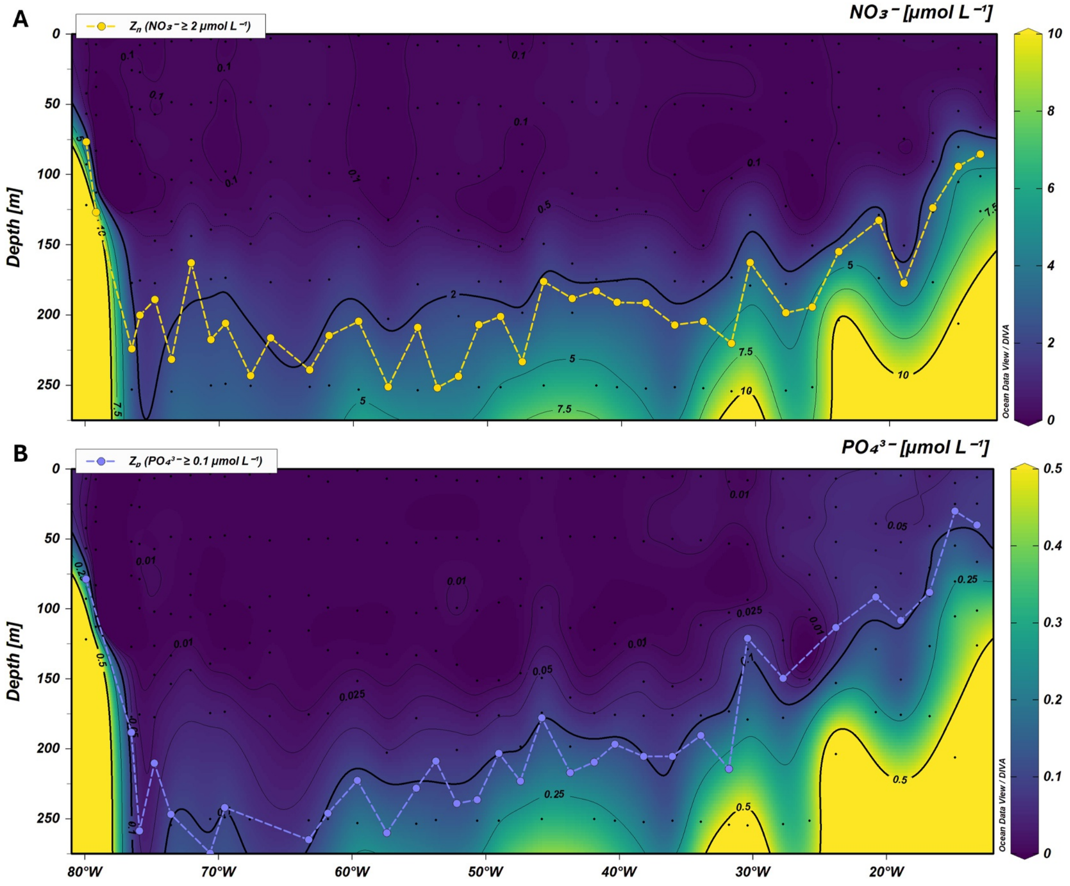

Figure 4. Cross-section plots of concentrations (in µmol L^{-1}) of (a) nitrate (NO_3^-), with yellow dashed line and dots indicating Z_N ($NO_3^- \geq 2$ µmol L^{-1}) and (b) phosphate (PO_4^{3-}), with blue dashed line and dots indicating Z_P ($PO_4^{3-} \geq 0.1$ µmol L^{-1}) at each station occupied across the transect. Black dots indicate discrete sampling depths.

Mixed-effects models including subregion as a random factor did not substantially improve explanatory power, suggesting that particulate stoichiometry is only weakly constrained by the measured environmental and biological variables at the basin scale.

In contrast, DOM C*:N was highly predictable (CV $R^2 = 0.91$; RMSE = 0.78). Stepwise regression identified DOP as the strongest single predictor (standardized coefficient $\beta = 34.0$). Random forest analysis pointed toward DOP as the dominant variable, followed by weaker contributions from PO_4^{3-} and microbial community composition metrics. Mixed-effects models nearly explained all variance in DOM C*:N (marginal $R^2 = 0.99$; conditional $R^2 = 0.997$), suggesting limited additional spatial structure beyond measured predictors. This suggests that DOM stoichiometry is most strongly associated with phosphorus availability, which was consistent across modeling approaches.

AC:HC ratios were also well explained (CV $R^2 = 0.86$; RMSE = 0.075; marginal $R^2 = 0.91$) by the environmental and biological predictor set. Across modeling approaches, *Prochlorococcus* abundance emerged as the strongest explanatory variable, while *Synechococcus*, temperature, and Hnac provided secondary explanatory power. Random forest results supported this ranking, with *Prochlorococcus* contributing the highest variable importance score (Table S2 in Supporting Information S1). This suggests that the AC:HC balance is primarily structured by cyanobacterial composition and modulated by temperature. Across all response variables, phosphorus availability and microbial community composition consistently emerged as key predictors, suggesting that carbon processing pathways in the NASG are mainly associated with underlying nutrient availability.

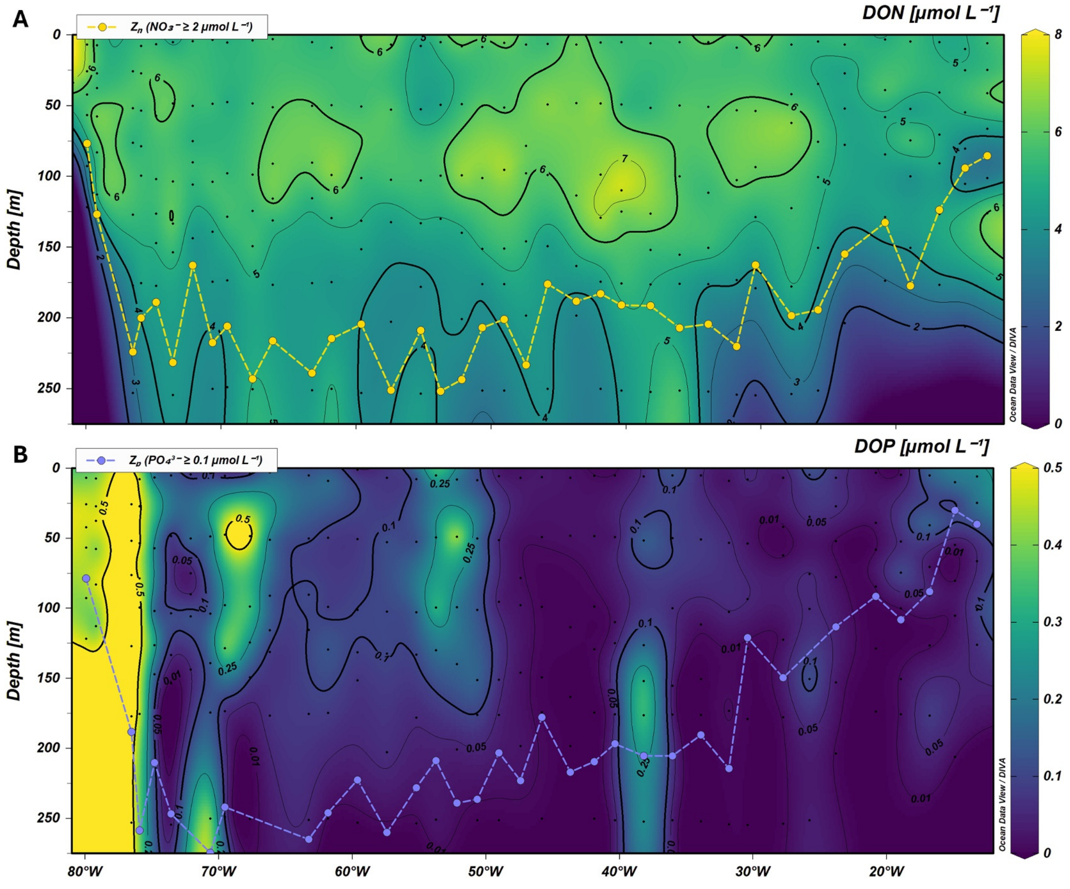

Figure 5. Cross-section plots of concentrations (in µmol L^{-1}) of (a) Dissolved organic nitrogen, with yellow dashed line and dots indicate Z_N ($NO_3^- \geq 2$ µmol L^{-1}) and (b) dissolved organic phosphorus, with blue dashed line and dots indicate Z_P ($PO_4^{3-} \geq 0.1$ µmol L^{-1}) across the transect. Black dots indicate discrete sampling depths.

Table 3
*Inventory of Particulate (POM), Dissolved (DOM), Total (TOM) Organic Matter, Total Stoichiometry (Dissolved Organic + Inorganic, Total N:P), and Semi-Conservative N_2-Fixation Tracer N**

	Western boundary (*n* = 2)	Western basin (*n* = 15)	Mid-Atlantic ridge (*n* = 8)	Eastern basin (*n* = 9)	Eastern boundary (*n* = 4)
POM C:N	5 ± −	8 ± 4	8 ± 2	8 ± 1	7 ± 1
POM N:P	44 ± 7	36 ± 18	25 ± 11	18 ± 2	20 ± 2
POM C:P	213 ± 14	212 ± 45	182 ± 46	149 ± 23	128 ± 10
DOM C*:N	21 ± −(11 ± −)	15 ± 6 (8 ± 3)	10 ± 3 (5 ± 1)	9 ± 2 (5 ± 1)	10 ± 2 (6 ± 1)
DOM N:P	14 ± −	39 ± 21	307 ± 214	184 ± 218	81 ± 45
DOMC*:P	298 ± 2	483 ± 155	2,479 ± 1,593	1,564 ± 1,621	792 ± 333
TOM N:P	16 ± −	42 ± 23	258 ± 170	79 ± 39	16 ± 3
Total N:P	14 ± 1	40 ± 22	281 ± 206	100 ± 72	35 ± 8
N*	2.6 ± 0.1	2.6 ± 0.1	2.7 ± 0.1	2.3 ± 0.3	1.8 ± 0.2

Note. For DOM, two estimates–C* inferred from global mean bulk DOM and (in parentheses) from mean semi-labile DOM stoichiometry–are given. Additional endmember DOM stoichiometries specific to the NASG are provided in Table S3 in Supporting Information S1. All data are depth-integrated and presented as mean ± SD per defined subregion.

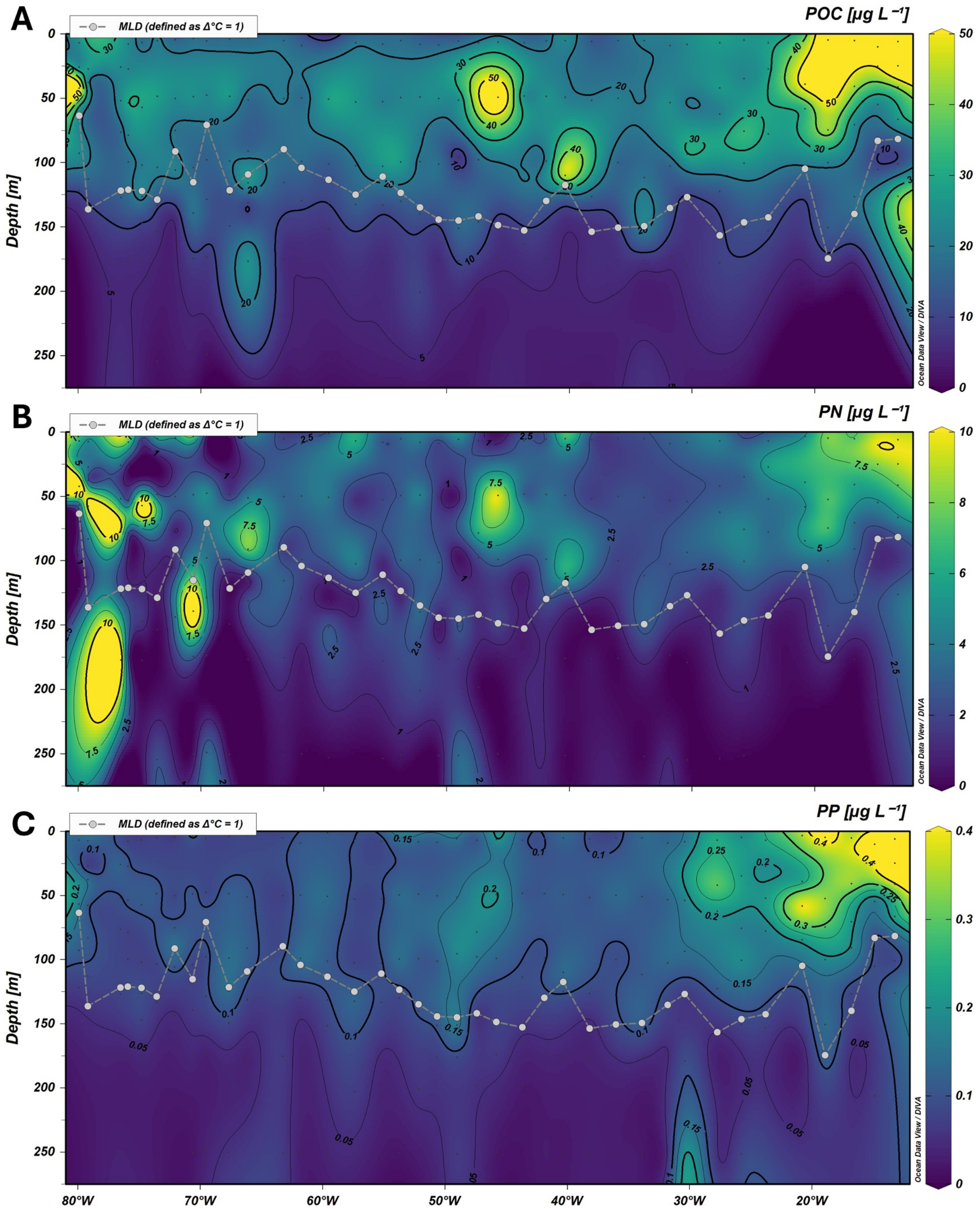

Figure 6. Cross-section plots of measured concentrations (in µg L^{-1}) of (a) Particulate organic carbon, (b) particulate organic nitrogen, and (c) Particulate phosphorus across the transect. Gray dashed lines and dots indicate the calculated mixed layer depth at each station occupied, and black dots indicate discrete sampling depths.

4. Discussion

4.1. Controls on the Hydrography of the Subtropical North Atlantic

The high-resolution data set presented here (∼2° station spacing), combined with statistical analysis of physico-chemical and biological parameters, provides a detailed view of the hydrographic structure across the subtropical North Atlantic between 23° and 27°N, particularly the NASG. Hydrogeography is strongly influenced by basin-scale circulation, notably the AMOC, which modulates heat transport and stratification (Primeau, 2005; Smeed et al., 2018). Consistent with this framework, we observed a west-east gradient of decreasing temperature and increasing salinity, reflecting the advection of colder, saline waters transported into the NASG interior and the impact of eastern boundary upwelling systems.

Stratification was evident in the mean MLD (125 ± 25 m) and associated density structure, consistent with other oligotrophic gyres in the Pacific and Indian Oceans. Long-term observations indicate that global warming has been associated with increased gyre stratification (~6.1% since the 1960s (Yamaguchi & Suga, 2019)), and is expected to further expand (Polovina et al., 2008), partly linked to AMOC weakening (Smeed et al., 2018). Deep nutriclines across most of the transect indicate restricted vertical nutrient supply, with shoaling confined to the gyre margins.

These patterns align with the nutrient-ratio budget framework of Xiang et al. (2023), where stratification not only limits nutrient input but systematically shapes nutrient imbalances that structure ecological communities. Our observations confirm that circulation-driven stratification acts as a first-order control on both physical structure and nutrient limitation in the NASG.

4.2. Diverging Nutrient Regimes Across the Subtropical North Atlantic

The subtropical North Atlantic exhibits strong basin-scale contrasts in nutrient availability. While Gulf Stream influence in the west and the Mauritanian upwelling in the east provide episodic nutrient inputs (Williams et al., 2011, 2026), the gyre interior remains extremely depleted in surface NO_3^- (<50 nmol L^{-1}) and PO_4^{3-} (<10 nmol L^{-1}). These concentrations are consistent with previous observations (Martiny et al., 2019; Zubkov et al., 2007) and typify oligotrophic gyres globally, although the ultimately limiting nutrient might differ among basins (Browning & Moore, 2023; Moore et al., 2013).

Phosphorus availability appears particularly important in this system. Although Saharan dust (~193.5 Tg yr^{-1}) delivers substantial nutrient inputs to the subtropical Atlantic (Jickells et al., 2005), >85% of its phosphorus is insoluble and minimally bioavailable (Mahowald et al., 2008). In contrast, the iron-rich deposition can promote diazotrophic activity (Conway & John, 2014; Tagliabue et al., 2017), consistent with the high N_2-fixation observed in the NASG (~250 μmol N m^{-2} d^{-1}) (Capone et al., 2005), rates substantially higher than in the Pacific gyres (30–120 μmol N m^{-2} d^{-1}) (Mahaffey et al., 2014). Observed N* anomalies are consistent with potential enhanced diazotrophic influence, likely from *Trichodesmium* and UCYN-A (Breitbarth et al., 2007; S. E. Reynolds et al., 2007). High concentrations of DON (>7 μmol L^{-1}) near the Mid-Atlantic Ridge further suggest coupling between trace metal supply and increased N_2-fixation (Kunde et al., 2019; Tuerena et al., 2019). We emphasize, however, that N* values are indirect indicators and can also reflect physical transport or remineralization processes (Williams et al., 2026). Consequently, although elevated DON in the gyre interior is consistent with positive N* anomalies, these observations may reflect a combination of biological production and physical processes, and interpretations of diazotrophy should be considered with caution in the absence of direct N_2-fixation measurements.

In the absence of equivalent phosphorus inputs, nitrogen fixation contributes to sustained P-stress, increasing reliance on DOP as an alternative nutrient source (Dhyrman, 2016; Mahaffey et al., 2014; S. Reynolds et al., 2014). Observed DOP concentrations (210 ± 160 nmol L^{-1} in the western NASG) are consistent with previously reported values (210 ± 10 nmol L^{-1} reported for the eastern basin) (Mather et al., 2008). DOP remains an important phosphorus resource under chronic PO_4^{3-} depletion. Our statistical models independently indicated a strong statistical association ($\beta = 34.0$; marginal $R^2 = 0.99$; CV $R^2 = 0.91$) between DOP and DOM across the basin.

4.3. Factors Determining the Microbial Community in the Subtropical North Atlantic

Microbial community structure broadly tracked hydrographic and nutrient gradients. *Prochlorococcus* dominated the oligotrophic gyre interior, exceeding cell counts of *Synechococcus* by up to five-fold, while *Synechococcus* and picoeukaryotes increased toward nutrient-enriched eastern waters. This partitioning is consistent with global cyanobacterial biogeography (Flombaum et al., 2013) and reflects combined nutrient and temperature controls. Our modeling supports this mechanistic interpretation: autotroph:heterotroph biomass ratios (AC:HC) were strongly associated with *Prochlorococcus* abundance (marginal $R^2 = 0.91$; CV $R^2 = 0.86$), with additional contributions from temperature and Hnac bacteria. These results confirm that phytoplankton composition is a primary determinant of trophic structure across the transect.

Adaptations underpinning *Prochlorococcus* dominance–genome streamlining, ecotype partitioning, and small cell size–facilitate survival in ultraoligotrophic waters (Casey et al., 2022; Luo, 2015; Painter et al., 2014). In contrast, *Synechococcus* exhibits greater metabolic plasticity and responsiveness to nutrient pulses (Scanlan et al., 2009).

Heterotrophic bacteria showed analogous partitioning: Lnac bacteria dominated the stratified interior of the NASG, while Hnac bacteria increased in nutrient-replete boundary regions. *Prochlorococcus*-Lnac partnerships in the gyre interior and *Synechococcus*-Hnac associations at productive margins indicate tight coupling between microbial trophic structure and nutrient availability.

These structural differences imply contrasting carbon processing pathways. In *Prochlorococcus*-dominated, phosphorus-limited regions, elevated C:P production and enhanced recycling are consistent with greater retention and transformation of organic matter in the dissolved form (Jiao et al., 2010; Letscher & Moore, 2015; Liang et al., 2023). In contrast, boundary systems characterized by *Synechococcus* and picoeukaryote-rich communities are associated with conditions more conducive to POM production and export (Hopkinson & Vallino, 2005; Liang et al., 2023).

4.4. Impact of Community Structure on Organic Matter Stoichiometry

Organic matter stoichiometry closely tracked nutrient and community gradients. Elevated POM C:P (>200) and N:P (>35) ratios in the western NASG correspond well with reported cellular stoichiometry of *Prochlorococcus* (228 ± 77 C:P, 22 ± 9 N:P) and *Synechococcus* (188 ± 68 C:P, 21 ± 7 N:P) (Fagan et al., 2024; Lomas et al., 2021), consistent with strong phosphorus limitation in the gyre interior. Model results show that particulate C:N was only weakly predictable (CV $R^2 - 0.24$; marginal $R^2 = 0.054$), with PO_4^{3-}, *Prochlorococcus*, and Lnac identified as key predictors, indicating that particulate composition is strongly influenced by dynamic production and environmental variability, particularly in boundary regions.

In contrast, DOM C*:N was highly predictable and closely associated with DOP, suggesting a strong statistical relationship between phosphorus availability and inferred DOM composition. Central NASG waters exhibited elevated C*:N and C*:P relative to boundary regions and global averages (Table 3) (Hopkinson & Vallino, 2005; Jiao et al., 2010; Letscher & Moore, 2015; Liang et al., 2023).

DOM carbon (C*) in this study is a derived proxy based on DON and DOP using literature-based stoichiometric assumptions (Liang et al., 2023). As such, it does not represent direct DOC measurements and should be interpreted in a relative sense. Absolute values and derived C*:N and C*:P ratios are subject to uncertainty and are interpreted as indicative of relative DOM composition rather than quantitative carbon concentrations. To assess this uncertainty, C* was calculated using multiple DOM endmember compositions (global bulk, global semi-labile, and regionally constrained NASG bulk and semi-labile). Despite substantial variability in absolute values (Table S3 in Supporting Information S1), basin-scale spatial gradients were consistent across all assumptions. Coefficients of variation across endmembers ranged from ~30% to 50% for C*:N and ~70%–80% for C*:P, indicating that uncertainty is larger for P-normalized ratios but does not alter the observed spatial patterns. Importantly, these patterns are independently supported by directly measured N:P ratios, which show pronounced nitrogen enrichment relative to phosphorus in the gyre interior. This supports the interpretation of strong phosphorus stress and enhanced microbial processing (Jiao et al., 2010; Letscher & Moore, 2015), irrespective of the specific DOM stoichiometric assumption. While the C* approach does not allow precise quantification of DOM carbon concentration or lability, the combined evidence from measured nutrients and inferred stoichiometry indicates systematic differences in organic matter processing across the basin. Direct DOC measurements and molecular-level characterization would further refine these constraints.

Taken together, these results are consistent with a basin-scale functional gradient in organic matter processing, with enhanced recycling and accumulation of carbon-enriched DOM in the stratified gyre interior and comparatively greater particulate production in nutrient-influenced boundary regions. This gradient reflects the combined influence of stratification, nutrient limitation, and microbial community structure at basin-scale. The differing sensitivity of C*:N and C*:P to DOM endmember assumptions reflects the asymmetric biogeochemical control of nitrogen and phosphorus in oligotrophic systems. Low and highly variable phosphorus concentrations amplify uncertainty in P-normalized metrics, whereas nitrogen-based ratios remain comparatively more stable.

5. Conclusions and Broader Context

NASG combines features that distinguish it from other oligotrophic gyres. Like all subtropical gyres, it is permanently stratified with chronically low nutrient concentrations, yet it receives far greater dust inputs than the Pacific or Indian gyres (Jickells et al., 2005), stimulating diazotrophy at rates exceeding those observed elsewhere (Capone et al., 2005; Mahaffey et al., 2014). As a result, phosphorus limitation is particularly pronounced, situating the NASG among the more strongly P-stressed regions of the global ocean (Browning & Moore, 2023; Moore et al., 2013).

The microbial community is strongly structured by nutrient availability, with interior regions associated with more strongly recycled, phosphorus-poor organic matter (Jiao et al., 2010; Letscher & Moore, 2015), while boundary regions are associated with conditions supporting more labile organic matter production (Hopkinson & Vallino, 2005). Statistical analyses confirm that microbial composition and nutrient availability jointly structure organic matter pools across the basin. Although the transect reflects late winter conditions, spatial gradients in nutrient limitation and community composition are consistent with long-term observations (Martiny et al., 2019; Zubkov et al., 2007), suggesting that these patterns are robust beyond seasonal variability. Given ongoing climate-driven changes, including stratification intensification and potential circulation weakening, the balance between dissolved and particulate matter pathways may shift, with implications for carbon cycling efficiency in the North Atlantic. Finally, this study highlights the importance of integrating physical, chemical, and biological measurements to resolve coupled biogeochemical processes at basin scales.

Conflict of Interest

The authors declare no conflicts of interest relevant to this study.

Availability Statement

The data presented in this study is made available in Supporting Information S1, JC191 cruise data is available at CCHDO under expocode 740H20200119 (https://cchdo.ucsd.edu/cruise/740H20200119).

Acknowledgments
The authors wish to thank the crew and scientific personnel of the RSS James Cook and specifically chief scientist Alejandra Sanchez-Franks. This work was part of the UK contribution to the GO-SHIP program, and supported by the University of Portsmouth Faculty of Science and Health PhD bursary scheme, and a NERC CLASS ECR Fellowship.

References

Becker, S., Aoyama, M., Woodward, E. M. S., Bakker, K., Coverly, S., Mahaffey, C., & Tanhua, T. (2020). GO-SHIP repeat hydrography nutrient manual: The precise and accurate determination of dissolved inorganic nutrients in seawater, using continuous flow analysis methods. *Frontiers in Marine Science*, *7*, 581790. https://doi.org/10.3389/fmars.2020.581790

Breitbarth, E., Oschlies, A., & LaRoche, J. (2007). Physiological constraints on the global distribution of Trichodesmium–effect of temperature on diazotrophy. *Biogeosciences*, *4*(1), 53–61. https://doi.org/10.5194/bg-4-53-2007

Browning, T. J., & Moore, C. M. (2023). Global analysis of ocean phytoplankton nutrient limitation reveals high prevalence of co-limitation. *Nature Communications*, *14*(1), 5014. https://doi.org/10.1038/s41467-023-40774-0

Cai, L., Li, H., Deng, J., Zhou, R., & Zeng, Q. (2024). Biological interactions with Prochlorococcus: Implications for the marine carbon cycle. *Trends in Microbiology*, *32*(3), 280–291. https://doi.org/10.1016/j.tim.2023.08.011

Calvo-Díaz, A., Díaz-Pérez, L., Suárez, L. Á., Morán, X. A. G., Teira, E., & Marañón, E. (2011). Decrease in the autotrophic-to-heterotrophic biomass ratio of picoplankton in oligotrophic marine waters due to bottle enclosure. *Applied and Environmental Microbiology*, *77*(16), 5739–5746. https://doi.org/10.1128/aem.00066-11

Capone, D. G., Burns, J. A., Montoya, J. P., Subramaniam, A., Mahaffey, C., Gunderson, T., et al. (2005). Nitrogen fixation by Trichodesmium spp.: An important source of new nitrogen to the tropical and subtropical North Atlantic Ocean. *Global Biogeochemical Cycles*, *19*(2). https://doi.org/10.1029/2004gb002331

Casey, J. R., Boiteau, R. M., Engqvist, M. K. M., Finkel, Z. V., Li, G., Liefer, J., et al. (2022). Basin-scale biogeography of marine phytoplankton reflects cellular-scale optimization of metabolism and physiology. *Science Advances*, *8*(3). https://doi.org/10.1126/sciadv.abl4930

Conway, T. M., & John, S. G. (2014). Quantification of dissolved iron sources to the North Atlantic Ocean. *Nature*, *511*(7508), 212–215. https://doi.org/10.1038/nature13482

Dave, A. C., Barton, A. D., Lozier, M. S., & McKinley, G. A. (2015). What drives seasonal change in oligotrophic area in the subtropical North Atlantic? *Journal of Geophysical Research: Oceans*, *120*(6), 3958–3969. https://doi.org/10.1002/2015jc010787

Davis, C. B., Blackbird, S., Wolff, G., Woodward, M., & Mahaffey, C. (2019). Seasonal organic matter dynamics in a temperate shelf sea. *Progress in Oceanography*, *177*, 101925. https://doi.org/10.1016/j.pocean.2018.02.021

Davis, C. E., Mahaffey, C., Wolff, G. A., & Sharples, J. (2014). A storm in a shelf sea: Variation in phosphorus distribution and organic matter stoichiometry. *Geophysical Research Letters*, *41*(23), 8452–8459. https://doi.org/10.1002/2014gl061949

de Boyer Montégut, C., Madec, G., Fischer, A. S., Lazar, A., & Iudicone, D. (2004). Mixed layer depth over the global ocean: An examination of profile data and a profile-based climatology. *Journal of Geophysical Research*, *109*(C12). https://doi.org/10.1029/2004jc002378

Dickson, A. G., Sabine, C. L., & Christian, J. R. (2007). *Guide to best practices for ocean CO2 measurements*. North Pacific Marine Science Organization.

Dyhrman, S. T. (2016). Nutrients and their acquisition: Phosphorus physiology in microalgae. *The physiology of microalgae*, 155–183.

Fagan, A. J., Tanioka, T., Larkin, A. A., Lee, J. A., Garcia, N. S., & Martiny, A. C. (2024). Elemental stoichiometry of particulate organic matter across the Atlantic Ocean. *Biogeosciences*, *21*(19), 4239–4250. https://doi.org/10.5194/bg-21-4239-2024

Flombaum, P., Gallegos, J. L., Gordillo, R. A., Rincón, J., Zabala, L. L., Jiao, N., et al. (2013). Present and future global distributions of the marine Cyanobacteria Prochlorococcus and Synechococcus. *Proceedings of the National Academy of Sciences*, *110*(24), 9824–9829. https://doi.org/10.1073/pnas.1307701110

Friedlingstein, P., O'Sullivan, M., Jones, M. W., Andrew, R. M., Hauck, J., Landschützer, P., et al. (2024). Global Carbon Budget 2024. *Earth System Science Data Discussions*, 1–133.

Gruber, N., & Sarmiento, J. L. (1997). Global patterns of marine nitrogen fixation and denitrification. *Global Biogeochemical Cycles*, *11*(2), 235–266. https://doi.org/10.1029/97gb00077

Guidi, L., Chaffron, S., Bittner, L., Eveillard, D., Larhlimi, A., Roux, S., et al. (2016). Plankton networks driving carbon export in the oligotrophic ocean. *Nature*, *532*(7600), 465–470. https://doi.org/10.1038/nature16942

Hickman, A. E., Dutkiewicz, S., Williams, R. G., & Follows, M. J. (2010). Modelling the effects of chromatic adaptation on phytoplankton community structure in the oligotrophic ocean. *Marine Ecology Progress Series*, *406*, 1–17. https://doi.org/10.3354/meps08588

Hopkinson, C. S., Jr., & Vallino, J. J. (2005). Efficient export of carbon to the deep ocean through dissolved organic matter. *Nature*, *433*(7022), 142–145. https://doi.org/10.1038/nature03191

Jiao, N., Herndl, G. J., Hansell, D. A., Benner, R., Kattner, G., Wilhelm, S. W., et al. (2010). Microbial production of recalcitrant dissolved organic matter: Long-term carbon storage in the global ocean. *Nature Reviews Microbiology*, *8*(8), 593–599. https://doi.org/10.1038/nrmicro2386

Jickells, T. D., An, Z. S., Andersen, K. K., Baker, A. R., Bergametti, G., Brooks, N., et al. (2005). Global iron connections between desert dust, ocean biogeochemistry, and climate. *Science*, *308*(5718), 67–71. https://doi.org/10.1126/science.1105959

Kara, A. B., Rochford, P. A., & Hurlburt, H. E. (2003). Mixed layer depth variability over the global ocean. *Journal of Geophysical Research*, *108*(C3). https://doi.org/10.1029/2000jc000736

Knap, A. H., Michaels, A., Close, A. R., Ducklow, H., & Dickson, A. G. (1996). *Protocols for the joint global ocean flux study (JGOFS) core measurements* (Vol. 1994). JGOFS, Reprint of the IOC Manuals and Guides No. 29, UNESCO

Kunde, K., Wyatt, N. J., González-Santana, D., Tagliabue, A., Mahaffey, C., & Lohan, M. C. (2019). Iron distribution in the subtropical North Atlantic: The pivotal role of colloidal iron. *Global Biogeochemical Cycles*, *33*(12), 1532–1547. https://doi.org/10.1029/2019gb006326

Kwak, S. G., & Kim, J. H. (2017). Central limit theorem: The cornerstone of modern statistics. *Korean Journal of Anesthesiology*, *70*(2), 144. https://doi.org/10.4097/kjae.2017.70.2.144

Kwon, E. Y., Sreeush, M. G., Timmermann, A., Karl, D. M., Church, M. J., Lee, S. S., & Yamaguchi, R. (2022). Nutrient uptake plasticity in phytoplankton sustains future ocean net primary production. *Science Advances*, *8*(51), eadd2475. https://doi.org/10.1126/sciadv.add2475

Letscher, R. T., & Moore, J. K. (2015). Preferential remineralization of dissolved organic phosphorus and non-Redfield DOM dynamics in the global ocean: Impacts on marine productivity, nitrogen fixation, and carbon export. *Global Biogeochemical Cycles*, *29*(3), 325–340. https://doi.org/10.1002/2014gb004904

Liang, Z., Letscher, R. T., & Knapp, A. N. (2023). Global patterns of surface ocean dissolved organic matter stoichiometry. *Global Biogeochemical Cycles*, *37*(12), e2023GB007788. https://doi.org/10.1029/2023gb007788

Lomas, M. W., Baer, S. E., Mouginot, C., Terpis, K. X., Lomas, D. A., Altabet, M. A., & Martiny, A. C. (2021). Varying influence of phytoplankton biodiversity and stoichiometric plasticity on bulk particulate stoichiometry across ocean basins. *Communications Earth & Environment*, *2*(1), 143. https://doi.org/10.1038/s43247-021-00212-9

Lomas, M. W., Burke, A. L., Lomas, D. A., Bell, D. W., Shen, C., Dyhrman, S. T., & Ammerman, J. W. (2010). Sargasso Sea phosphorus biogeochemistry: An important role for dissolved organic phosphorus (DOP). *Biogeosciences*, *7*(2), 695–710. https://doi.org/10.5194/bg-7-695-2010

Luo, H. (2015). Evolutionary origin of a streamlined marine bacterioplankton lineage. *The ISME Journal*, *9*(6), 1423–1433. https://doi.org/10.1038/ismej.2014.227

Macovei, V. A., Torres-Valdés, S., Hartman, S. E., Schuster, U., Moore, C. M., Brown, P. J., et al. (2019). Temporal variability in the nutrient biogeochemistry of the surface North Atlantic: 15 years of ship of opportunity data. *Global Biogeochemical Cycles*, *33*(12), 1674–1692. https://doi.org/10.1029/2018gb006132

Mahaffey, C., Reynolds, S., Davis, C. E., & Lohan, M. C. (2014). Alkaline phosphatase activity in the subtropical ocean: Insights from nutrient, dust and trace metal addition experiments. *Frontiers in Marine Science*, *1*, 73. https://doi.org/10.3389/fmars.2014.00073

Mahowald, N., Jickells, T. D., Baker, A. R., Artaxo, P., Benitez-Nelson, C. R., Bergametti, G., et al. (2008). Global distribution of atmospheric phosphorus sources, concentrations and deposition rates, and anthropogenic impacts. *Global Biogeochemical Cycles*, *22*(4). https://doi.org/10.1029/2008gb003240

Martiny, A. C., Lomas, M. W., Fu, W., Boyd, P. W., Chen, Y. L. L., Cutter, G. A., et al. (2019). Biogeochemical controls of surface ocean phosphate. *Science Advances*, *5*(8), eaax0341. https://doi.org/10.1126/sciadv.aax0341

Masuda, T., Inomura, K., Mareš, J., Kodama, T., Shiozaki, T., Matsui, T., et al. (2023). Coexistence of dominant marine phytoplankton sustained by nutrient specialization. *Microbiology Spectrum*, *11*(4), e04000-22. https://doi.org/10.1128/spectrum.04000-22

Mather, R. L., Reynolds, S. E., Wolff, G. A., Williams, R. G., Torres-Valdes, S., Woodward, E. M. S., et al. (2008). Phosphorus cycling in the North and South Atlantic Ocean subtropical gyres. *Nature Geoscience*, *1*(7), 439–443. https://doi.org/10.1038/ngeo232

Moore, C. M., Mills, M. M., Arrigo, K. R., Berman-Frank, I., Bopp, L., Boyd, P. W., et al. (2013). Processes and patterns of oceanic nutrient limitation. *Nature Geoscience*, *6*(9), 701–710. https://doi.org/10.1038/ngeo1765

Muratore, D., Gilbert, N. E., LeCleir, G. R., Wilhelm, S. W., & Weitz, J. S. (2025). Diel partitioning in microbial phosphorus acquisition in the Sargasso Sea. *Proceedings of the National Academy of Sciences*, *122*(11), e2410268122. https://doi.org/10.1073/pnas.2410268122

Painter, S. C., Patey, M. D., Tarran, G. A., & Torres-Valdés, S. (2014). Picoeukaryote distribution in relation to nitrate uptake in the oceanic nitracline. *Aquatic Microbial Ecology*, *72*(3), 195–213. https://doi.org/10.3354/ame01695

Polimene, L., Sailley, S., Clark, D., Mitra, A., & Allen, J. I. (2017). Biological or microbial carbon pump? The role of phytoplankton stoichiometry in ocean carbon sequestration. *Journal of Plankton Research*, *39*(2), 180–186.

Polovina, J. J., Howell, E. A., & Abecassis, M. (2008). Ocean's least productive waters are expanding. *Geophysical Research Letters*, *35*(3). https://doi.org/10.1029/2007gl031745

Primeau, F. (2005). Characterizing transport between the surface mixed layer and the ocean interior with a forward and adjoint global ocean transport model. *Journal of Physical Oceanography*, *35*(4), 545–564. https://doi.org/10.1175/jpo2699.1

R Core Team. (2022). *R: A language and environment for statistical computing*. R Foundation for Statistical Computing. Retrieved from https://www.R-project.org/

Reay, D. S., Dentener, F., Smith, P., Grace, J., & Feely, R. A. (2008). Global nitrogen deposition and carbon sinks. *Nature Geoscience*, *1*(7), 430–437. https://doi.org/10.1038/ngeo230

Reynolds, S., Mahaffey, C., Roussenov, V., & Williams, R. G. (2014). Evidence for production and lateral transport of dissolved organic phosphorus in the eastern subtropical North Atlantic. *Global Biogeochemical Cycles*, *28*(8), 805–824. https://doi.org/10.1002/2013gb004801

Reynolds, S. E., Mather, R. L., Wolff, G. A., Williams, R. G., Landolfi, A., Sanders, R., & Woodward, E. M. S. (2007). How widespread and important is N2 fixation in the North Atlantic Ocean? *Global Biogeochemical Cycles*, *21*(4). https://doi.org/10.1029/2006gb002886

Ridge, S. M., & McKinley, G. A. (2020). Advective controls on the North Atlantic anthropogenic carbon sink. *Global Biogeochemical Cycles*, *34*(7), e2019GB006457. https://doi.org/10.1029/2019gb006457

Scanlan, D. J., Ostrowski, M., Mazard, S., Dufresne, A., Garczarek, L., Hess, W. R., et al. (2009). Ecological genomics of marine picocyanobacteria. *Microbiology and Molecular Biology Reviews*, *73*(2), 249–299. https://doi.org/10.1128/mmbr.00035-08

Smeed, D. A., Josey, S. A., Beaulieu, C., Johns, W. E., Moat, B. I., Frajka-Williams, E., et al. (2018). The North Atlantic Ocean is in a state of reduced overturning. *Geophysical Research Letters*, *45*(3), 1527–1533. https://doi.org/10.1002/2017gl076350

Tagliabue, A., Bowie, A. R., Boyd, P. W., Buck, K. N., Johnson, K. S., & Saito, M. A. (2017). The integral role of iron in ocean biogeochemistry. *Nature*, *543*(7643), 51–59. https://doi.org/10.1038/nature21058

Tarran, G. A., & Bruun, J. T. (2015). Nanoplankton and picoplankton in the Western English Channel: Abundance and seasonality from 2007–2013. *Progress in Oceanography*, *137*, 446–455. https://doi.org/10.1016/j.pocean.2015.04.024

Tuerena, R. E., Williams, R. G., Mahaffey, C., Vic, C., Green, J. M., Naveira-Garabato, A., et al. (2019). Internal tides drive nutrient fluxes into the deep chlorophyll maximum over mid-ocean ridges. *Global Biogeochemical Cycles*, *33*(8), 995–1009. https://doi.org/10.1029/2019gb006214

Williams, R. G., Brown, P. J., Takano, Y., Forget, G., Jones, D., Katavouta, A., et al. (2026). The biogeochemical transport by the Gulf Stream. *Communications Earth & Environment*, *7*(1), 149. https://doi.org/10.1038/s43247-025-03118-y

Williams, R. G., McDonagh, E., Roussenov, V. M., Torres-Valdes, S., King, B., Sanders, R., & Hansell, D. A. (2011). Nutrient streams in the North Atlantic: Advective pathways of inorganic and dissolved organic nutrients. *Global Biogeochemical Cycles*, *25*(4). https://doi.org/10.1029/2010gb003853

Xiang, Y., Quay, P. D., Sonnerup, R. E., & Fassbender, A. J. (2023). Subtropical gyre nutrient cycling in the upper ocean: Insights from a nutrient-ratio budget method. *Geophysical Research Letters*, *50*(13), e2023GL103213. https://doi.org/10.1029/2023gl103213

Yamaguchi, R., & Suga, T. (2019). Trend and variability in global upper-ocean stratification since the 1960s. *Journal of Geophysical Research: Oceans*, *124*(12), 8933–8948. https://doi.org/10.1029/2019jc015439

Zubkov, M. V., Mary, I., Woodward, E. M. S., Warwick, P. E., Fuchs, B. M., Scanlan, D. J., & Burkill, P. H. (2007). Microbial control of phosphate in the nutrient-depleted North Atlantic subtropical gyre. *Environmental Microbiology*, *9*(8), 2079–2089. https://doi.org/10.1111/j.1462-2920.2007.01324.x